X-734-69-501

X-63799

TIME-OPTIMAL CONTROL OF GRAVITY GRADIENT SATELLITES WITH DISTURBANCES

FRANZ ZACH

NOVEMBER 1969

GODDARD SPACE FLIGHT CENTER
GREENBELT, MARYLAND

30

X-734-69-501

TIME-OPTIMAL CONTROL OF GRAVITY GRADIENT SATELLITES WITH DISTURBANCES

Franz Zach

November 1969

GODDARD SPACE FLIGHT CENTER
Greenbelt, Maryland

CONTENTS

TIME-OPTIMAL CONTROL OF GRAVITY GRADIENT SATELLITES WITH DISTURBANCES*

ABSTRACT

The optimal control of spacecraft with gravity gradient coarse stabilization and active libration damping for precision pointing represents a promising approach for advanced experiments, e.g. laser communications, where angular position within .001° must be achieved and maintained in the presence of disturbances. This paper deals with the time optimal control for this case. A suboptimal (i.e. nearly optimal) control law for the general gravity gradient satellite (GGS) is obtained by a two-step approximation: first the general GGS is approximated by a dumbbell satellite (DS) and secondly a small angle approximation is derived. The optimal control law for this case is calculated and applied to two representative examples of a 24 hour synchronous GGS. The practical results are shown and discussed. It can be seen how the optimal control law derived for the DS works for the general GGS as a suboptimal control law. The Maximum Principle, which is used in this paper, is also extended to cover operating conditions with disturbances. It is shown that disturbances change the optimal control law significantly, a result that is very important for practical applications of the maximum principle.

*The work for this paper was accomplished while the author held a National Research Council Postdoctoral Resident Research Associateship supported by the National Aeronautics and Space Administration, Goddard Space Flight Center. The author is very much obliged to Mr. W. Isley and Mr. D. Endres for their valuable suggestions.

NOMENCLATURE

The center of all coordinate systems are at the center of mass (c.m.) of the spacecraft. All coordinate systems are right handed.

a_x, a_y, a_z – gravity gradient coefficient for pitch, roll and yaw respectively

C_1 – linear viscous damping coefficient of the damper rod

C_2 – linear spring coefficient of the damper rod

$d_{(i)}$ – reduced disturbance torque ($= T_{di} / I_{ii}$), i = x, y, z

DS – Dumbbell Satellite

GG – Gravity Gradient

GGS – Gravity Gradient Satellite

H_{ib} – inertial angular momentum of the main body of the spacecraft, measured in body-fixed coordinates, i = x, y, z

I_r – moment of inertia of the damper rod about its axis of rotation

I_b – inertia tensor of the main spacecraft body

r – distance from the center of the earth to the c.m. of the spacecraft

t – time

$T_{c(i)}$ – control torques, i = x, y, z

$T_{d(i)}$ – disturbance torques, i = x, y, z

U_i – reduced control torques ($= T_{ci}/I_{ii}$), i = x, y, z

$\vec{v}$ – inertial velocity of the spacecraft

x_0, y_0, z_0 – attitude reference system (x_0 has the direction from the center of the earth to the c.m. of the spacecraft, y_0 lies normal to x_0 and in the orbital plain such that the component of $\vec{v}$ in the y_0 direction is greater than zero)

x_b, y_b, z_b – coordinate system fixed to the main body of the spacecraft (x_b – yaw axis, y_b – roll axis, z_b – pitch axis)

x_d, y_d, z_d – coordinate system fixed to the damper rod

– pitch angle

– set value of pitch angle

– earth gravitational constant

$_{ib}$ – orbital angular rate, i.e. rotation of the x_0, y_0, z_0 system in inertial space, measured in the x_b, y_b, z_b system, i = x, y, z

$_1$ $_2$ – angles of the damper rod relative to the body – fixed coordinate system

– time consumed for damping of initial librations

– roll angle

$_s$ – set value of roll angle

– yaw angle

$_{ib}$ – angular inertial velocity of the main body of the spacecraft, measured in the x_b, y_b, z_b – system, i = x, y, z

$_0$ – orbital angular rate for a circular orbit ($= \mu / r^3$)

TIME-OPTIMAL CONTROL OF GRAVITY GRADIENT SATELLITES WITH DISTURBANCES*

1. INTRODUCTION

The development of control policies for highly precise fine pointing of spacecraft is a necessary condition for a number of advanced experiments, e.g. laser communications. The gravity gradient technique [1,2] offers a good approach for long term coarse stabilization of a spacecraft. However, precise pointing to certain angles is required for some experiments, and it may be desirable to accomplish this in minimum time. Also for these experiments, disturbances such as the solar torque acting on the spacecraft must be counteracted by proper control.

The overall optimal control policy must meet two basic objectives: (1) acquisition of the precision pointing mode in minimum time starting from a coarse GG mode, and (2) extended term precision pointing by counteraction of disturbance torques. This paper will treat only the acquisition requirement. The optimal control law as developed herein is applied to two representative examples of a synchronous equatorial 24 hour earth spacecraft. The method employed for active libration damping is the use of a reaction jet device operating in the micro-pound thrust level regime, which can be an ion engine, resistojet, or pulsed plasma system. It is envisioned that any use of the ion engine would require special consideration of control actuations. The main difficulty with the ion engine is that it cannot be readily turned on and off for thrusting purposes. One possibility is to combine libration damping with orbit corrections. Another possibility is to

provide a balanced couple which cancels out the orbital effects. The resistojet [3] has already been studied as a means of optimal large angle maneuvering for a synchronous spacecraft. Pulsed plasma systems appear to offer high promise for use in both acquisition and holding modes due to their precision impulse bit capability and relatively high specific impulse. It is assumed that a minimum of six thrust directions is provided on the spacecraft to provide control in pitch, roll, and yaw axes.

The procedure used to develop these control laws is as follows:

1. The general rotational equations of motion for a GGS including a damping mechanism is formulated.
2. These equations are linearized for a DS in a circular equatorial orbit with small libbrations.
3. The optimal control laws are developed for this DS. To check the validity of these control laws for a more general synchronous GGS, the control laws are applied to the simulation of the complete GGS.

2. EQUATIONS OF MOTION FOR A GRAVITY GRADIENT SATELLITE

For development of an optimal control law, a GGS which has four rigid GG booms and a rigid damper rod is assumed.

The damper rod will be assumed to rotate in a plane fixed with respect to the main body. The spacecraft-damper rod system therefore represents a seven degree of freedom system. For pointing the axes of the spacecraft to given angles only the equations of rotational motion are of interest for circular orbits. These are

$$\cdot \mathbf{I} \begin{pmatrix} \dot{\Omega}_{xb} \\ \dot{\Omega}_{yb} \\ \dot{\Omega}_{zb} \end{pmatrix} \quad \begin{pmatrix} \Omega_{xb} \\ \Omega_{yb} \\ \Omega_{zb} \end{pmatrix} \cdot \tag{1}$$

where

$$\begin{aligned} \cdot_{xb} \quad & \mathbf{M}_{xb} \cdot \mathbf{M}_{xd} \sin \cdot_2 \cdot \mathbf{M}_{zd} \cos \cdot_2 - (\Omega_{yb} \mathbf{H}_{zb} - \Omega_{zb} \mathbf{H}_{yb}) - \mathbf{P} \cos \cdot_2 \cdot \mathbf{T}_{cx} \cdot \mathbf{T}_{dx} \cdot \\ \cdot_{yb} \quad & \mathbf{M}_{yb} \cdot \mathbf{M}_{xd} \cos \cdot_2 \cos \cdot_1 \cdot \mathbf{M}_{SD} \sin \cdot_1 \cdot \mathbf{M}_{zd} \sin \cdot_2 \cos \cdot_1 - (\Omega_{zb} \mathbf{H}_{xb} - \Omega_{xb} \mathbf{H}_{zb}) \\ & \cdot \mathbf{P} \sin \cdot_2 \cos \cdot_1 \cdot \mathbf{T}_{cy} \cdot \mathbf{T}_{dy} \end{aligned} \tag{2}$$

and

$$\begin{aligned} \cdot_{zb} \quad & \mathbf{M}_{zb} \cdot \mathbf{M}_{xd} \cos \cdot_2 \sin \cdot_1 - \mathbf{M}_{SD} \cos \cdot_1 \cdot \mathbf{M}_{zd} \sin \cdot_2 \sin \cdot_1 - (\cdot_{xb} \mathbf{H}_{yb} - \cdot_{yb} \mathbf{H}_{xb}) \\ & \cdot \mathbf{P} \sin \cdot_2 \sin \cdot_1 \cdot \mathbf{T}_{cz} \cdot \mathbf{T}_{dz} \cdot \end{aligned}$$

The torques M_{ib} and M_{id} caused by the gravity gradient effect are: for the main body of the spacecraft

$$\left.\begin{aligned} \mathbf{M}_{xb} \quad & - \frac{3\mu}{r^3} [(\mathbf{I}_{yy} - \mathbf{I}_{zz}) a_2 a_3 + \mathbf{I}_{xy} a_1 a_3 - \mathbf{I}_{xz} a_1 a_2 + \mathbf{I}_{yz} (a_3^2 - a_2^2)] \cdot \\ \mathbf{M}_{yb} \quad & - \frac{3\mu}{r^3} [(\mathbf{I}_{zz} - \mathbf{I}_{xx}) a_1 a_3 - \mathbf{I}_{xy} a_2 a_3 \cdot \mathbf{I}_{xz} (a_1^2 - a_3^2) + \mathbf{I}_{yz} a_1 a_2] \end{aligned}\right\}$$

and

$$\left.\begin{aligned} \mathbf{M}_{zb} \quad & - \frac{3\mu}{r^3} [(\mathbf{I}_{xx} - \mathbf{I}_{yy}) a_1 a_2 + \mathbf{I}_{xy} (a_2^2 - a_1^2) + \mathbf{I}_{xz} a_2 a_3 - \mathbf{I}_{yz} a_1 a_3] \end{aligned}\right\} \tag{3}$$

and for the damper rod

$$\left.\begin{aligned} \mathbf{M}_{xd} \quad & 0 \cdot \\ \mathbf{M}_{yd} \quad & - \frac{3\mu}{r^3} \mathbf{I}_\ell \, b_1 \, b_2 \cdot \\ \mathbf{M}_{zd} \quad & - \frac{3\mu}{r^3} \mathbf{I}_\ell \, b_1 \, b_3 \end{aligned}\right\}$$

and

P and M_{SD} used in (2) are given by:

$$\left.\begin{aligned} P &= I_{\quad xd}(\quad yd \quad \quad 2) \\ M_{SD} &= C_1 \quad 2 + C_2 \quad 2 \end{aligned}\right\} \qquad (4)$$

and

where the latter term is the restoring torque exerted on the damper rod by the spring-damper mechanism.

The a_i (i = 1, 2, 3) and b_i (i = 1, 2, 3) used in (3), which give the relations of the GG torques to the angular positions, are:

$$\left.\begin{aligned} a_1 &= \cos \quad \cos \quad \\ a_2 &= \cos \quad \sin \quad \sin \quad - \sin \quad \cos \quad \\ a_3 &= -\cos \quad \sin \quad \cos \quad + \sin \quad \sin \quad \\ b_1 &= a_1 \sin \quad_2 + a_2 \cos \quad_2 \cos \quad_1 + a_3 \cos \quad_2 \sin \quad_1 \\ b_2 &= -a_2 \sin \quad_1 + a_3 \cos \quad_1 \end{aligned}\right\} \qquad (5)$$

and

$$b_3 = a_1 \cos \quad_2 - a_2 \sin \quad_2 \cos \quad_1 - a_3 \sin \quad_2 \sin \quad_1$$

The equation of motion for the damper rod is

$$\ddot{\quad}_2 = -\dot{\Omega}_{yb} \sin \quad_1 + \dot{\Omega}_{zb} \cos \quad_1 - \Omega_{zd} \quad_{xd} - \frac{M_{yd} + M_{SD}}{I_{\quad}} \qquad (6)$$

Integration of (1) and (6) furnishes Ω_{xb}, Ω_{yb}, Ω_{zb} and $\quad_2$.

The pitch, roll, and yaw angles, which are the Euler angles between the body-fixed and the attitude reference system, will be used throughout this report. These can be obtained by subtracting $\vec{\xi}_b$, the orbital rate which is the rate at which the attitude reference system rotates in the inertial system, from $\vec{\Omega}_b$.

This gives

$$\left.\begin{aligned} &\frac{1}{\cos\ }\left(\quad_{yb}-\quad_{yb}\right)\sin\ \cdot\ \cdot\ \cdot\ _{zb}-\quad_{zb}\right)\cos\ \cdot\ \cdot \\ &\cdot\ \cdot\ \left(\quad_{yb}-\quad_{yb}\right)\cos\ \cdot\ \cdot\ \cdot\ _{xb}-\quad_{zb}\right)\sin\ \cdot \\ &\cdot\ \cdot\ _{xb}-\quad_{yb}\ \cdot\ \sin\ \cdot\ \cdot \end{aligned}\right\} \qquad (7)$$

and

A digital program was written[1] which allows the calculation of , , , , and $_2$ according to Equations (1) through (7). This program also pays attention to elastic collision processes of the damper rod against its stops, which limit the rotation of the damper rod in the $x_1 - z_1$ plane.

3. APPROXIMATION OF GRAVITY GRADIENT SATELLITES BY A DUMBBELL SATELLITE

In this section the equations of motion for a DS will be derived from the equations developed in the previous section for that of the more general gravity gradient satellite (GGS). Thus it will be assumed that no damper rod exists, that I_{yy} and I_{zz} are the same order of magnitude, and that

$$I_{yy} \quad I_{zz} \quad I_{xx} \qquad (8)$$

Eq. (1) and (2) now yield:

$$\left.\begin{aligned} &I_{xx}\ _{xb}\ (I_{yy}-I_{zz})\ _{yb}\ _{zb}-T_{cx}-T_{dx}-M_{xb} \qquad (a) \\ &I_{yy}\ _{yb}\ (I_{zz}-I_{xx})\ _{zb}\ _{xb}-T_{cy}-T_{dy}-M_{yb} \qquad (b) \end{aligned}\right\} \qquad (9)$$

and

$$I_{zz}\ _{zb}\ (I_{xx}-I_{yy})\ _{xb}\ _{yb}-T_{cz}-T_{dz}-M_{zb} \qquad (c)$$

Equation (3) becomes:

$$\left.\begin{aligned} M_{xb} &= -\frac{3\mu}{r^3}(I_{yy} - I_{zz})\, a_2\, a_3 \\ M_{yb} &= -\frac{3\mu}{r^3}(I_{zz} - I_{xx})\, a_1\, a_3 \\ M_{zb} &= -\frac{3\mu}{r^3}(I_{xx} - I_{yy})\, a_1\, a_2 \end{aligned}\right\} \qquad (10)$$

and

$$M_{xd} = M_{yd} = M_{zd} = 0 \,.$$

For small angles Equations (9) and (10) can be approximated[4] by:

$$\left.\begin{aligned} \ddot{\phi} - \omega_0^2 \frac{I_{zz} - I_{yy}}{I_{xx}}\,\psi - \frac{I_{zz} - I_{yy} - I_{xx}}{I_{xx}}\,\omega_0\,\dot{\psi} &= \frac{T_{cx} + T_{dx}}{I_{xx}} \quad (a) \\ \ddot{\psi} - 4\,\omega_0^2 \frac{I_{zz} - I_{xx}}{I_{yy}}\,\psi - \frac{I_{zz} - I_{xx} - I_{yy}}{I_{yy}}\,\omega_0\,\dot{\phi} &= \frac{T_{cy} + T_{dy}}{I_{yy}} \quad (b) \end{aligned}\right\} \qquad (11)$$

and

$$\ddot{\theta} - 3\,\omega_0^2 \frac{I_{yy} - I_{xx}}{I_{zz}}\,\theta = \frac{T_{cz} + T_{dz}}{I_{zz}} \,. \qquad (c)$$

where $\omega_0^2 = \mu / r^3 = \omega_{zb}^2$ and $\omega_{xb} = \omega_{yb} = 0$ for nearly circular equatorial orbit. The sign on the right side of Equation (11b) is changed with respect to Equation (9b); this only means that torques about the y axis are considered negative. This approach leads to a more convenient form for the derivation of the following optimal control concepts.

It is now assumed that

$$I_{zz} = I_{yy} + I_{xx} \,. \qquad (12)$$

as is true, e.g. for the ATS-D and ATS-E spacecraft. Thus Eq. (11) become

$$\ddot{\phi} = a_x \omega_0^2 u_x - d_x \tag{13}$$

$$\ddot{\theta} = a_y \omega_0^2 u_y - d_y \tag{14}$$

and

$$\ddot{\psi} = a_z \omega_0^2 u_z - d_z \tag{15}$$

where

$$a_x = \frac{I_{zz} - I_{yy}}{I_{xx}}$$

$$a_y = 4 \frac{I_{zz} - I_{xx}}{I_{yy}}$$

$$a_z = 3 \frac{I_{yy} - I_{xx}}{I_{zz}}$$

$$u_x = \frac{T_{cx}}{I_{xx}}, \quad u_y = \frac{T_{cy}}{I_{yy}}, \quad u_z = \frac{T_{cz}}{I_{zz}}$$

$$d_x = \frac{T_{dx}}{I_{xx}}, \quad d_y = \frac{T_{dy}}{I_{yy}} \text{ and } d_z = \frac{T_{dz}}{I_{zz}}$$

When $d_x = d_y = d_z = 0$ and u_x, u_y, u_z are constant each of the Equations (13) to (15) obviously gives circles for each of the phase plane plots $(\phi, \dot{\phi})$, $(\theta, \dot{\theta})$ or $(\psi, \dot{\psi})$ respectively. Simulations of the GGS under the same conditions result in circles for the phase plane plots (trajectories) for angles up to 10°. This also proves the applicability of the approximations used to obtain these equations.

4. OPTIMAL CONTROL FOR THE DUMBBELL SATELLITE

Equations (13), (14), and (15) give a set of decoupled equations for pitch, yaw and roll angles of a D.S. These equations make the derivation of an optimal

control law using Pontryagin's Maximum Principle practically feasible. It is assumed that the reduced control torques u_x, u_y and u_z are bounded in magnitude, i.e.

$$\left.\begin{aligned} -K_x \leq u_x \leq K_x \\ -K_y \leq u_y \leq K_y \\ -K_z \leq u_z \leq K_z \end{aligned}\right\} \qquad (16)$$

and

4.1 Optimal Control Laws for Pitch (α) with no Disturbance Torques

Let

$$\left.\begin{aligned} x_1 &= \alpha \\ x_2 &= \dot{\alpha} \end{aligned}\right\} \qquad (17)$$

and

Thus (14) becomes

$$\left.\begin{aligned} \dot{x}_1 &= x_2 \\ \dot{x}_2 &= -ax_1 - u_y \end{aligned}\right\} \qquad (18)$$

when $d_y = 0$.

The theory of optimal control [5, 6] shows that a vector

$$\vec{p} = \begin{bmatrix} p_1 \\ \\ p_2 \end{bmatrix}$$

is used to calculate the dot product

$$H = \vec{p} \cdot \dot{\vec{x}} \qquad (19)$$

where

$$\dot{\vec{x}} \quad \begin{bmatrix} \dot{x}_1 \\ \\ \dot{x}_2 \end{bmatrix}$$

Next (19) must be maximized by a proper choice of u_α.

Eq. (19) yields

$$H \quad p_1 x_2 + p_2 (- a_\alpha x_1 + u_\alpha) .$$

which is maximized by

$$u_\alpha \quad K_\alpha \operatorname{sgn} p_2 \tag{20}$$

The theory of optimal control shows further, that

$$\frac{dp_i}{dt} \quad - \frac{\partial H}{\partial x_i} \quad i \quad 1, 2$$

which yields

and

$$\left.\begin{aligned} \dot{p}_1 &\quad - a_\alpha p_2 \\ \dot{p}_2 &\quad - p_1 \end{aligned}\right\} \tag{21}$$

Solving (21) gives

$$\vec{p} \quad \begin{bmatrix} - A \sqrt{a_\alpha} \cos (\sqrt{a_\alpha} t - \varphi) \\ \\ A \sin (\sqrt{a_\alpha} t - \varphi) \end{bmatrix} \tag{22}$$

where A, $\varphi > 0$ are integration-constants. Eq. (20) can now be written as:

$$u_\alpha = K_\alpha \operatorname{sgn}\left[\sin\left(\sqrt{a_\alpha}\,t - \varphi\right)\right]. \tag{23}$$

The solution of (18) is then:

$$\left.\begin{aligned} x_1(t) &= \frac{\pm K_\alpha}{a_\alpha} + \left(x_{10} - \frac{\pm K_\alpha}{a_\alpha}\right)\cos\sqrt{a_\alpha}\,t + \frac{x_{20}}{\sqrt{a_\alpha}}\sin\sqrt{a_\alpha}\,t \\ \text{and} \\ \frac{x_2(t)}{\sqrt{a_\alpha}} &= -\left(x_{10} - \frac{\pm K_\alpha}{a_\alpha}\right)\sin\sqrt{a_\alpha}\,t + \frac{x_{20}}{\sqrt{a_\alpha}}\cos\sqrt{a_\alpha}\,t \end{aligned}\right\} \tag{24}$$

where

$$x_{10} = x_1\,(t = 0)$$

and

$$x_{20} = x_2\,(t = 0) = \dot{x}_1\,(t = 0)$$

It can be seen that $x_1(t)$ and $x_2(t)/\sqrt{a_\alpha}$ form a circle in the $x_1(t) - x_2(t)/\sqrt{a_\alpha}$ - plane.

The center of this circle lies at

$$x = \frac{K_\alpha}{a_\alpha} \text{ for } u_\alpha = K_\alpha$$

and at

$$x = -\frac{K_\alpha}{a_\alpha} \text{ for } u_\alpha = -K_\alpha .$$

To find the optimum switching law we first consider initial conditions (x_{10}, x_{20}), which lie on a circle which passes through the origin. Comparing Eq. (23) and (24), it is clear that optimal trajectories cannot stay longer than for an

angle $\sqrt{a_\alpha}\, t = \pi$ on a specific circle. Therefore one can obtain the geometric locus of all points with initial conditions (x_{10}, $x / \sqrt{a_\alpha} = 0$), which can be transferred immediately into the origin, to be the two semi-circles shown in Fig. 2.

Now assume initial conditions which require at least two switching points according to Eq. (23). Also assume the last trajectory will lie on S_{-1}. Eq. (23) and (24) show, that the next to the last state with $u_\alpha = + K_\alpha$ must last for

$$t = \frac{\pi}{\sqrt{a_\alpha}}$$

It can be seen further, that this state is represented by a semicircle with its origin at K_α / a_α, with its endpoint on S_{-1} and its starting point at a semicircle with its origin at $3\, K_\alpha / a_\alpha$ and a radius of K_α / a_α (see Fig. 3 and Ref. 5 and 6). When we apply this procedure for all such states leading to S_{-1}, we see that the switching circle for switching from $- K_\alpha$ to $+ K_\alpha$ is given by another semicircle with its center at $3\, K_\alpha / a_\alpha$ and a radius of K_α / a_α. When we continue this procedure for all initial conditions in the $x_1 - x_2 / \sqrt{a_\alpha}$ plane, we see that the switching circles are located as in Fig. 3.

Therefore the centers of the switching circles are located at

$$(2n - 1)\frac{K_\alpha}{a}, \quad n = \cdots -2, -1, 0, 1, 2 \cdots, \tag{25}$$

where n is the number of the switching circle.

4.2 Optimal Control Laws for Roll ( ) and Yaw ( ) with no Disturbance Torques

When Eq. (13), (14), and (15) are compared, no difference in their form is noted as long as $a_{\cdot} \neq 0$, $a_{\cdot} \neq 0$ and $a_{\cdot} \neq 0$. This is valid for a spacecraft with different principal moments of inertia. Therefore for this case the same optimal control law can be applied to Roll and Yaw as is derived for Pitch in Section 4.1. This is obtained by substituting $(a_{\cdot}, K_{\cdot})$ by $(a_{\cdot}, K_{\cdot})$ or $(a_{\cdot}, K_{\cdot})$ respectively. However, another control law must be derived, when two or three of the principle moments of inertia are equal. This will be done in the next section for yaw, when $I_{yy} = I_{zz}$.

The flow chart of a digital program for the control laws developed in this section and section 4.1 is given in Fig. 4. In this program a deadband is defined as

$$= \sqrt{x_1^2 + \left(\frac{x_2}{\sqrt{a_1}}\right)^2}$$

with $a_1 = a_{\cdot}, a_{\cdot}$ or $a_{\cdot}$ respectively.

Control is switched off completely, when the state of the system is inside this deadband (loop 1). Disturbances or later the application of the exact GGS – program can drive the system out of the deadband again (loop 2).

4.3 Optimal Control Law for Yaw (ψ) for $I_{yy} = I_{zz}$ with no Disturbance Torques

For a symmetrical spacecraft $I_{yy} = I_{zz} >> I_{xx}$ and hence a_{ψ} becomes 0. For this case another optimal control law must be derived for yaw (ψ):

Let

$$\left.\begin{aligned} x_1 &= -1 \\ x_2 &= -1 \end{aligned}\right\} \tag{26}$$

and

then (12) becomes

$$\left.\begin{aligned} \dot{x}_1 &= x_2 \\ \dot{x}_2 &= u_b \end{aligned}\right\} \tag{27}$$

and

Using (19) and (26) the Hamiltonian becomes $H = p_1 x_2 + p_2 u_b$, which is maximized by

$$u_b = K_b \operatorname{sgn} p_2 .$$

Applying

$$\frac{dp_i}{dt} = -\frac{\partial H}{\partial x_i} \quad (i = 1, 2)$$

again gives

$$\left.\begin{aligned} \dot{p}_1 &= 0 \\ \dot{p}_2 &= -p_1 \end{aligned}\right\} \tag{28}$$

and

which results in

$$\left.\begin{aligned} p_1 &= B \\ p_2 &= -Bt + C \end{aligned}\right\} \tag{29}$$

and

From Eq. (27) and (29) one obtains

$$\left.\begin{aligned} x_1 &= K_b \frac{t^2}{2} \operatorname{sgn} (C - Bt) + Dt + E \\ x_2 &= K_b\, t \operatorname{sgn} (C - Bt) + D \end{aligned}\right\} \tag{30}$$

and

Thus all trajectories are parabolas. From (29) it is evident, that p_2 can change sign at most once. Therefore the complete optimal trajectory from a given initial condition in the $x_1 - x_2$ - plane consists of one or two segments of a parabola, where the second parabola leads to the origin. It is evident, that the parabolas leading to the origin are also the switching lines (see Fig. 5 and Ref. 5 and 6).

For initial conditions with $x_{20} = 0$ the time consumed for reaching the origin can be calculated to be

$$\tau = 2\sqrt{\frac{x_{20}}{K_\psi}}$$

Figure 6 shows the flow chart for a digital program of this control law.

4.4 Consideration of Different Reference Values

The optimal control laws in the above sections lead α , Φ and ψ to the origin. We will now consider the case for reference values (set values) α_s , Φ_s , $\psi_s \neq 0$. Considering Eq. (13) through (15) with a_α , a_Φ , $a_\psi \neq 0$ one sees that the following new equations can be written, which contain an additional control term of thrust to balance the gravity gradient torque at the set value:

$$\left.\begin{aligned} \ddot{\psi} + a_\psi \psi &= \pm K_\psi + a_\psi \psi_s \\ \ddot{\Phi} + a_\Phi \Phi &= \pm K_\Phi + a_\Phi \Phi_s \\ \ddot{\alpha} + a_\alpha \alpha &= \pm K_\alpha + a_\alpha \alpha_s \end{aligned}\right\} \qquad (31)$$

and

But Eq. (31) also can be written as

$$\ddot{\psi}_1 + a_\psi \psi_1 = \pm K_\psi ,$$

$$\ddot{\Phi}_1 + a_\Phi \Phi_1 = \pm K_\Phi$$

and

$$\ddot{\alpha}_1 + a_\alpha \alpha_1 = + K_\alpha ,$$

where

$$\psi_1 = \psi - \psi_s$$

$$\phi_1 = \phi - \phi_s$$

and

$$\alpha_1 = \alpha - \alpha_s .$$

Therefore Eq. (17) - (24) can be applied as before, now leading ψ_1, ϕ_1, and α_1 to 0 and therefore ψ, ϕ and α to the desired setpoints. In Fig. 3 the switching lines will shift and also the optimal trajectories. This results in Fig. 7.

A similar approach is valid for yaw (ψ) when $a_\psi = 0$. The switching lines of Fig. 5 must simply be shifted so that they lead to ψ_s.

4.5 Consideration of Disturbances

The spacecraft usually is subjected to various disturbances, which are different in magnitude and time history. However, there are two typical kinds of disturbances, which should be considered: a constant bias torque and a disturbance torque with a 24 hour period. A constant disturbance torque can be caused e.g., by attitude thruster misalignments: station keeping thrusters can introduce disturbance torques where the thrust vector is not aligned through the center of mass. A disturbance torque with a 24 hr. period is caused, e.g. by solar pressure acting on the synchronous spacecraft.

First a constant disturbance torque will be considered. Eq. (15) now is

$$\ddot{\alpha} + a_\alpha \alpha = u_\alpha + d_\alpha , \qquad (32)$$

where d_a is the constant disturbance torque divided by I_{zz}. There are two approaches to solve this problem theoretically. First d_a could be measured by observing the shift of the trajectories and then counteracted by a control torque of the same magnitude. The total reduced control torque would be now:

$$u_a = \frac{T_{cz}}{I_{zz}} = + K_a - d_a \quad . \tag{33}$$

This would lead to the same switching lines for optimal control as in Fig. 2, 3 and 7. However the practical hardware constraints show that control torques according to Eq. (33) are much more difficult to implement than control torques of the form

$$\frac{T_{cz}}{I_{zz}} = \pm K_a \quad .$$

Therefore a modification of the switching lines of Fig. 2, 3 and 7 is found as follows:

From (32) one proceeds as was done for (17) - (22):

$$\dot{x}_1 = x_2,$$

$$\dot{x}_2 = - a_a x_1 + u_a + d_a$$

and

$$H = p_1 x_2 + p_2 (- a_a x_1 + u_a + d_a)$$

which again results in condition (23).

Substituting $\pm K_z$ by $\pm K_z + d_z$ in Equation (24) shows that all trajectories are shifted by d_z / a_z in the direction of the x_1-axis and that the radii change. Similar considerations which led to Figure 2 and 3 give Fig. 8 for the optimal switching lines.

Similar considerations hold for optimal control of . when a = 0. We only have to substitute $\pm K_{\_}$ by $\pm K_{\_} + d$ in Eq. (30). The equations for the switching lines read now:

$$\left.\begin{array}{l} x_2 \quad \sqrt{2(-K_{\_} - d)\, x} \quad \text{for } x_1 \geq 0 \\ \text{and} \\ x_2 \quad -\sqrt{2(K_{\_} - d)\, x_1} \quad \text{for } x_1 \leq 0 \end{array}\right\} \qquad (34)$$

It is obvious, that the above calculations are only valid for $K_{\_} > d_i$ for i = , , .

For slowly changing disturbances optimal control could be implemented by changing the switching lines according to Fig. 8 and according to the momentary value of d_i. The interactions of changing disturbances and changing of switching lines bring up serious problems of identification of disturbances and problems of stability, which are presently under investigation. Two approaches to optimal control while the disturbance torque is varying are shown in Fig. 9. It is assumed that the optimal trajectory starts without disturbance at x_{10}, $x_{20}/\sqrt{a}$ and reaches S_+^* and P_1 and follows S_+ (after switching control from $-K$ to $+K$) until a disturbance d occurs at the instant the state is at P_2. The trajectory now changes from that of S_+ to S_{d+}, where S_{d+} depends upon the disturbance. The S_{d+} trajectories are circles with their origin shifted by d/a in direction of x . Two procedures now exist:

*$S_{\_}$ replaces S_0, $S_{\_}$ replaces S_{-1} in section 4.1

a. Retention of + K at P_2, thereby following trajectory R_{d+} to P_3 and there switching to - K. When S_{d+} is reached at P_4, control is switched back to + K and S_{d+} followed to the origin, or

b. After occurence of the disturbance d at P_2, control is switched immediately to - K, until S_{d+} is reached at P_3'. S_{d+} then is followed to the origin by changing the control back to + K.

However, for the further investigations of the optimal control law in this paper it is assumed, that $T_d \ll K$ for all three axes. Thus, it is not necessary to apply the refined control law given in Fig. 8 and 9. The approach to the origin in presence of small disturbances can be seen from Fig. 10.

It can be seen from Fig. 10, that the positive x_1 axis may serve as an additional switching line when the trajectory intersects from the negative x_2 direction. The negative x_1 – axis forms the additional switching line in the case when the trajectory intersects coming from positive x_2 -values. A more sophisticated control law in the presence of disturbances is suggested for future work in this area as follows: switching from + K to - K or vice versa shall be implemented, when the distance from the set point (here the origin) starts to increase. This should at least give stable performance under all working conditions.

5. APPLICATION OF THE DS-OPTIMAL-CONTROL TO THE GRAVITY GRADIENT SATELLITE

This section will discuss the results of applying the DS control to the GGS computer simulation. Two GGS – configurations are used. The first, which will be called GGS 1, is characterized by $I_{yy} = I_{zz} \gg I_{xx}$ and no damping mechanism, the second (GGS 2) is characterized by the moments of inertia of the ATS-D satellite.

5.1 Data of the GGS

a. For the symmetric case (GGS 1)

$$I = \begin{bmatrix} 1000 & 0 & 0 \\ 0 & 48000 & 0 \\ 0 & 0 & 48000 \end{bmatrix} \text{ (in slug ft}^2\text{)}.$$

$I_z = 0$ and $C_1 = C_2 = 0$.

b. for the unsymmetric case (GGS 2)

$$I = \begin{bmatrix} 3180 & 0 & 0 \\ 0 & 13600 & 261 \\ 0 & 261 & 16700 \end{bmatrix} \text{ (in slug ft}^2\text{)}$$

$I_z = 540 \text{ slug ft}^2$.

$\varphi_1 = 53.4^0$.

$C_1 = 1.322 \text{ slug ft}^2/\text{sec}$

and

$C_2 = 4.7 \cdot 10^{-2} \text{ slug ft}^2/\text{sec}^2$.

5.2 Choice of Control Torques

In order to choose the proper magnitude of control torque it should be noted, that a necessary coidition for controllability of a gravity gradient satellite is, that in the whole pointing region for each axis

$$T_c \geq T_{gg} - T_d \qquad (35)$$

where T_c is the control torque exerted by the ion thruster, T_{gg} is the restoring torque due to the gravity gradient effect for a particular set of value and T_d is the disturbance torque. To point in a particular direction . . . a certain T_{gg} has to be counteracted; this torque can be calculated by Eq. (10). Since T_{gg} changes only when the set values of . . ., and . are changed and therefore much less often than T_d, counteraction of T_{gg} by a control torque of the same magnitude can be assumed. Pointing is desired to every point on the earth disc as seen from a synchronous spacecraft. Therefore -8.5° . . . 8.5° is valid, and a maximum gravity gradient torque in this region for the pitch ( ) - axis of the asymmetric spacecraft is given by

$$T_{gg\,\alpha\,max} \quad 2.5 \cdot 10^{-5} \text{ ft lb.}$$

A disturbance torque is assumed to be caused by solar pressure with a peak value of 10^{-5} ft #. Eq. (35) now yields

$$T_{c\alpha} \quad = 35 \cdot 10^{-6} \text{ ft lb.}$$

To give the same T_c/I ratios on the other axes of the asymmetric spacecraft and on all axes of the symmetric spacecraft, the following torques are chosen for the asymmetric spacecraft

$$T_{c\,\phi} = \pm 28.5 \cdot 10^{-6} \text{ ft lb}$$

and

$$T_{c\psi} = \pm 6.6 \cdot 10^{-6} \text{ ft lb.}$$

and for the symmetric spacecraft:

$$T_{c\alpha} = \pm 10^{-4} \text{ ft lb .}$$

$$T_{c\phi} = \pm 10^{-4} \text{ ft lb}$$

and

$$T_{c} = 2.09 \cdot 10^{-6} \text{ ft lb}$$

5.3 Comparison of Time Consumed for Damping Librations to $\dot{} = \dot{} = \dot{} = 0^{\circ}$ for GG Satellites and DS

The optimal switching lines given in Fig. 3, 5 and 7 are applied to all three axes simultaneously. To compare the results obtained for a GGS with the ideal case of a DS, the time consumed for reaching an angle of 0° after a certain initial condition is plotted in Fig. 11 and 12. For Fig. 11 the time consumed for a DS is calculated by applying the optimal control law derived in Section 4 to the equation $\ddot{x} + ax = u$ where $a = a_{z}$ and $u = \pm K_{z}$. Two different a_{z}, called a_{z1} and a_{z2} are used for GGS 1 and GGS 2, respectively. Therefore two different DS must be used for comparison. DS 1 uses a_{z1}, whereas DS 2 uses a_{z2}. The lower time consumed by a GGS for higher initial conditions can be explained as follows: the coupling of all three axes transfers some of the energy of the pitch axis to roll and yaw axes where optimal control is also being applied. Therefore energy is taken out of the whole system faster than for the uncoupled case of a DS. The region of $_{0}$ between 15° and 60° for GGS 2 shows on the other hand, that this effect is outweighed by the less exact approximation of an asymmetric GGS by a DS. Therefore a slightly higher time is consumed for this region than is predicted.

Figure 12 shows the equivalent comparisons for initial conditions $\neq 0$ only on roll ($_{0}$). Approximately the same a_{z} is used for both GGS 1 and GGS 2. Therefore approximately the same equivalent DS is valid for comparison of both GGS. Similar explanations for the shape of the plot hold as for pitch.

Since the yaw angle is not significant for pointing to certain points on the surface of the earth, plotting of the graphs for yaw equivalent to Fig. 11 and 12 are not given here. It is just mentioned, however, that for GGS 1 consistency with predicted values is achieved, whereas for GGS 2 some deviations of predicted values are observed. An exact explanation of this problem would involve a discussion of the exact equations (1) to (7) and goes beyond the scope of this paper.

5.4 Investigations of the Influence on the Settling Time of Initial Conditions not Equal to Zero on all Three Axes

To show the influence on of other initial conditions than in Section 5.3 $_0 = _0 = _0 \neq 0$ and $_0 = _0 = _0 = 0$ are chosen. Fig. 13 shows for pitch for GGS 1 and GGS 2 in comparison to the DS. Fig. 15 presents the graphs for roll. For yaw the same remarks are valid as in Section 5.3.

5.5 Pointing to Directions Other Than = = 0°

In the previous investigations, it always was assumed the pointing should lead to $_s = _s = 0°$. Now pointing to $_s$, $_s$ with $-8.5° \leq _s, _s \leq 8.5°$ is considered. The simulations show that application of the control law derived in Section 4.4 for reference values $\neq 0$ gives no difference in when pointed to set values $_s$, $_s$ other than $_s = _s = 0°$. This assumes that $_0 - _s$ or $_0 - _s$ now has the same value as $_0$ or $_0$ respectively in Sections 5.3 and 5.4. This assumes further that the same control torque T_c is still available and the torque necessary to counteract the gravity gradient torque T_{gg} at the set value is supplied in addition to T_c. is increased if counteracting of T_{gg} is provided by control thrust while decreasing the thrust T_c available for actual control purposes. Fig. 15 gives for the DS as a function of $K = T_c / I$. The parameter Θ is the difference between initial condition and the set value.

5.6 Influence of Disturbances on the Time Consumed (·) for Damping of Librations

Investigations concerning control under the influence of a sinusoidal disturbance torque with a 24 hour period were carried out. The peak value of T_d is assumed to be 10^{-5} ft lb. · is plotted in Fig. 16 for pitch ($_0 \neq 0$, $_0 = _0 = 0$) and in Fig. 17 for roll ($_0 \neq 0$, $_0 = _0 = 0$) with $_0 = _0 \quad _0 = 0$ in both cases.

Two phases for the disturbance torque are chosen, the first is 0° and the second is 180° relative to the starting point of control application.

It can be seen that under favorable phases of the disturbance torque the effect on control action nets in no increase of ·. One can also consider cases, where · could be decreased; whereas it can be seen from Fig. 16 and 17, that under unfavorable circumstances · is increased by 50%.

6. CLOSING REMARKS

It has been shown, that the time-optimal control law for a dumbbell satellite can be applied to a gravity gradient satellite as suboptimal control.

The next major consideration must be development of a control policy for the extended term precision pointing mode. Of special interest is the formulation of an adaptive disturbance torque computer for operation in a scallop mode limit cycle. It is also intended to expand the performance index for the acquisition mode to include both time and fuel weighting factors. Methods of state determination will also be assessed during follow-on application studies.

REFERENCES

1. Barrett, C. C., "The Development of a Mathematical Model and a Study of One Method of Orbit Adjust and Station Keeping Gravity-Oriented Satellites," TND-3652, Nov., 1966, NASA.

2. Roberson, R. E., "Attitude Control of Satellites and Space Vehicles," in: Advances in Space Sciences, Vol. 2, New York: Academic Press, Inc., 1960, pp. 351-436.

3. Isley, W. C., "Optimal Control Application for Electrothermal Multijet Systems on Synchronous Earth Spacecraft," Journal of Spacecraft and Rockets, Vol. 5, No. 12, Dec., 1968, pp. 1444-1451.

4. Frick, R. H., "Perturbations of a Gravity Gradient Stabilization System," Report AD 623279, The Rand Corporation, Santa Monica, California, Sept., 1965.

5. McCausland, I., "Introduction to Optimal Control," New York: John Wiley & Sons, Inc., 1969.

6. Jones, G. S., Strauss, A., Zvego, G. P., "Mathematical Aspects of Control Theory and the Problem of Satellite Attitude Control," NASA Contract NAS 5-9172, Final Report, January, 1966.

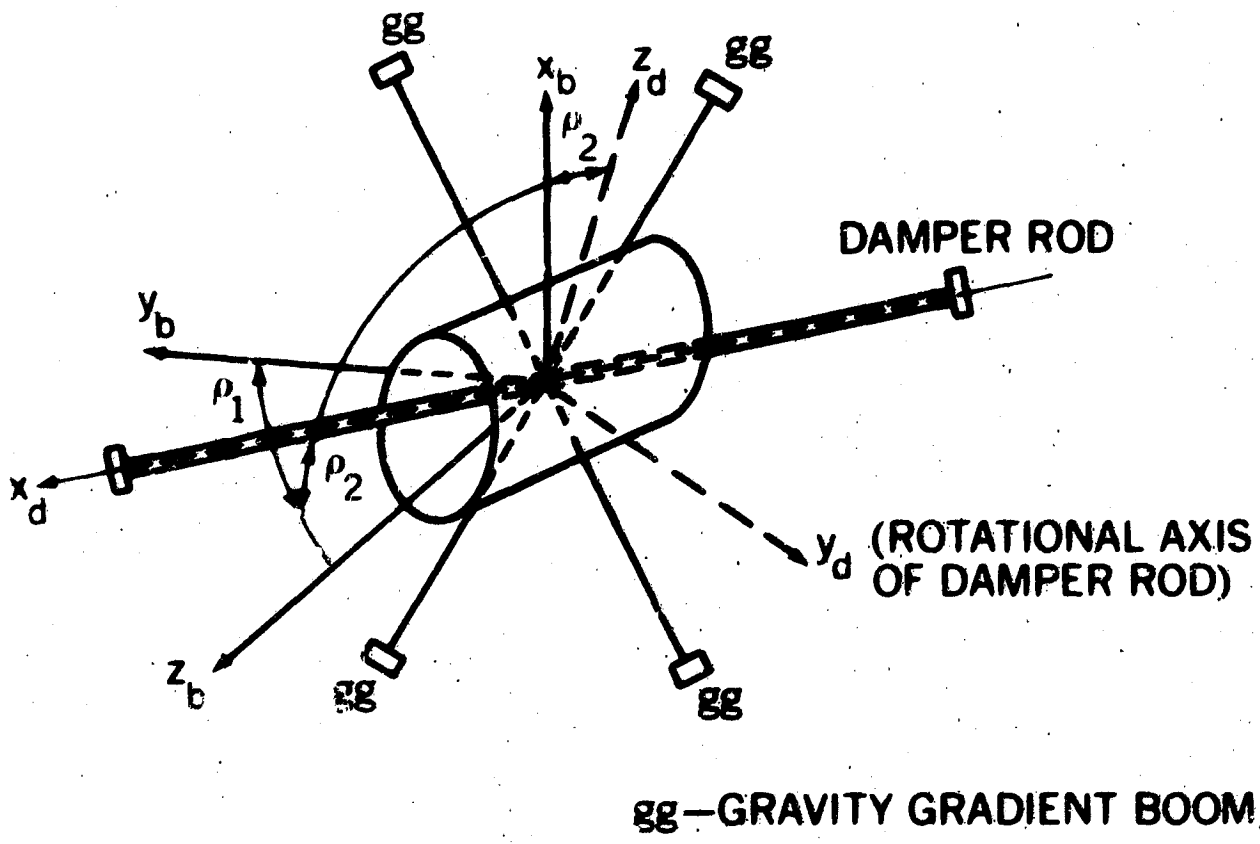

Figure 1—Gravity-gradient satellite x_b and y_b lie in the plane of the four booms and together with z_b establish a right-handed coordinate system fixed to the main body of the spacecraft. x_d, y_d, z_d establish a right-handed coordinate system fixed to the damper rod.

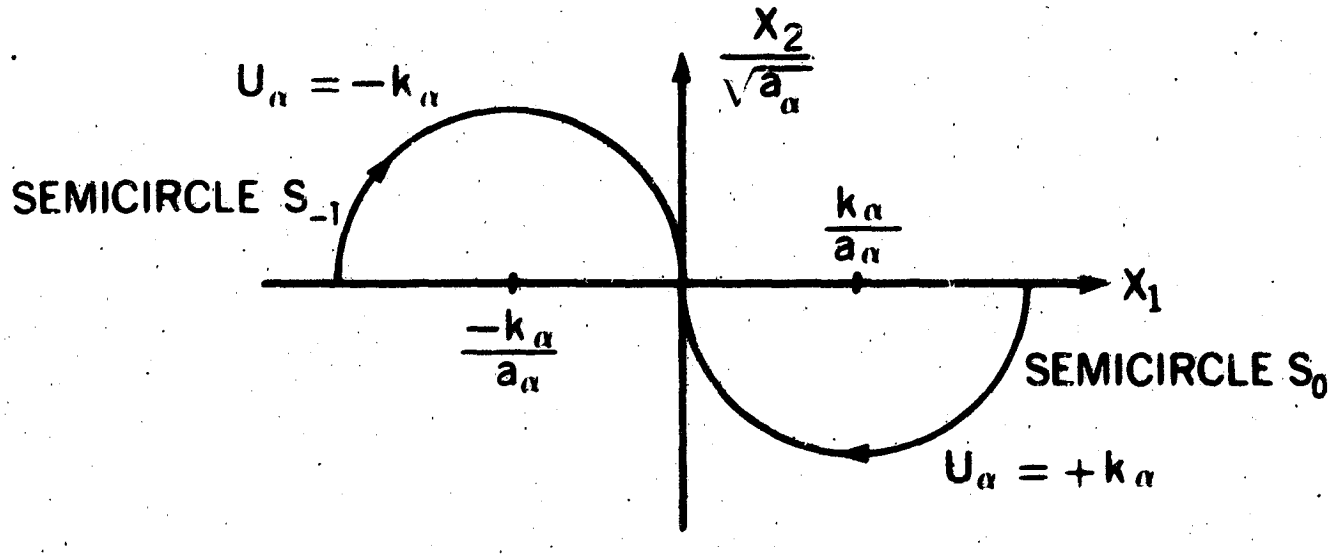

Figure 2–Geometric locus of all initial conditions x_{10}, x_{20}, $\overline{a_\alpha}$, which can be transferred to the origin immediately either by applying $+K_\alpha$ for S_0 or $-K_\alpha$ for S_{-1}.

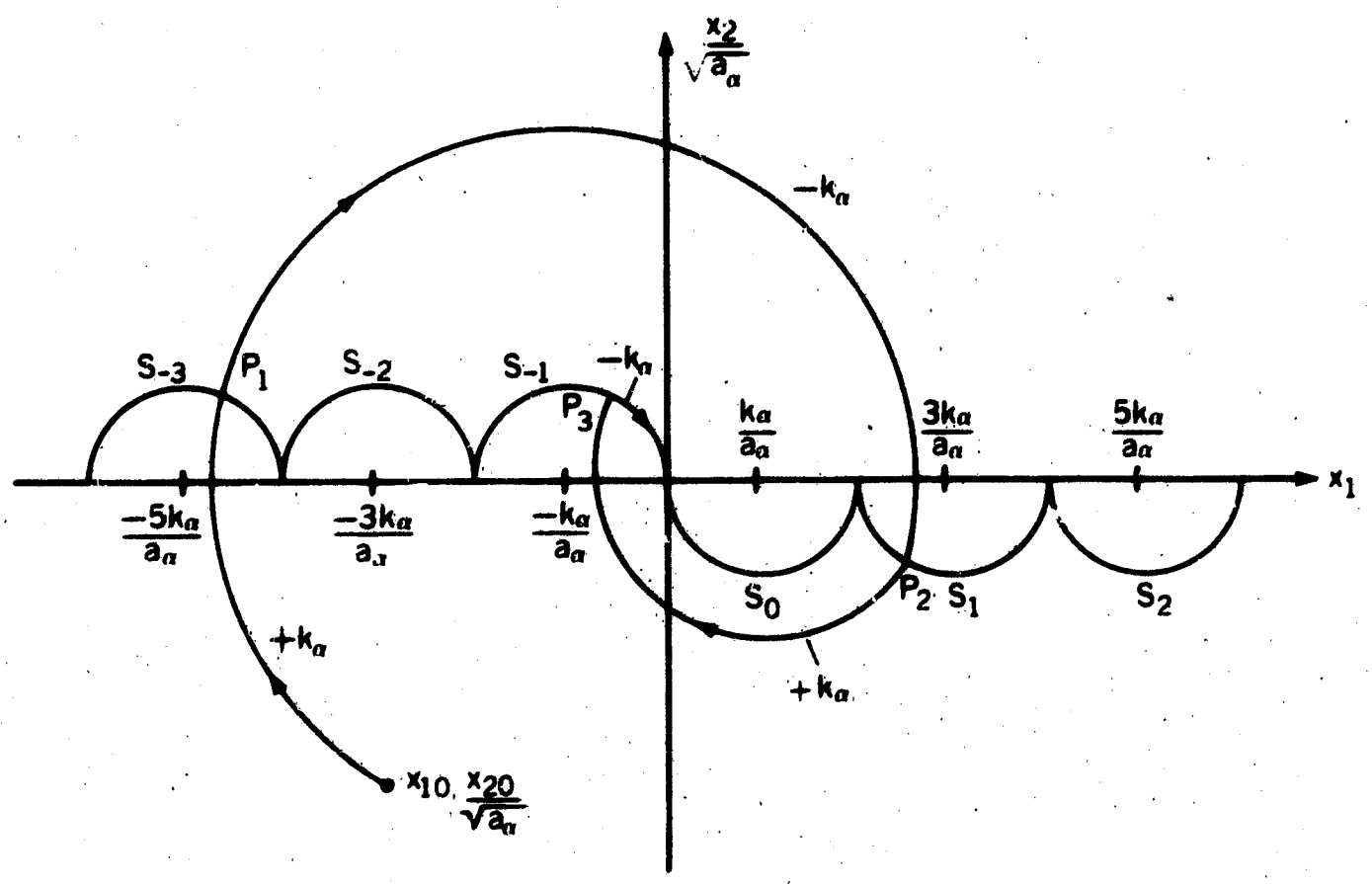

Figure 3–Switching lines S_{-3}, S_{-2}, S_{-1}, S_0, S_1, S_2, with a trajectory starting from (x_{10}, x_{20}, $\sqrt{a_\alpha}$). The switching points for the particular example illustrated are P_1, P_2 and P_3.

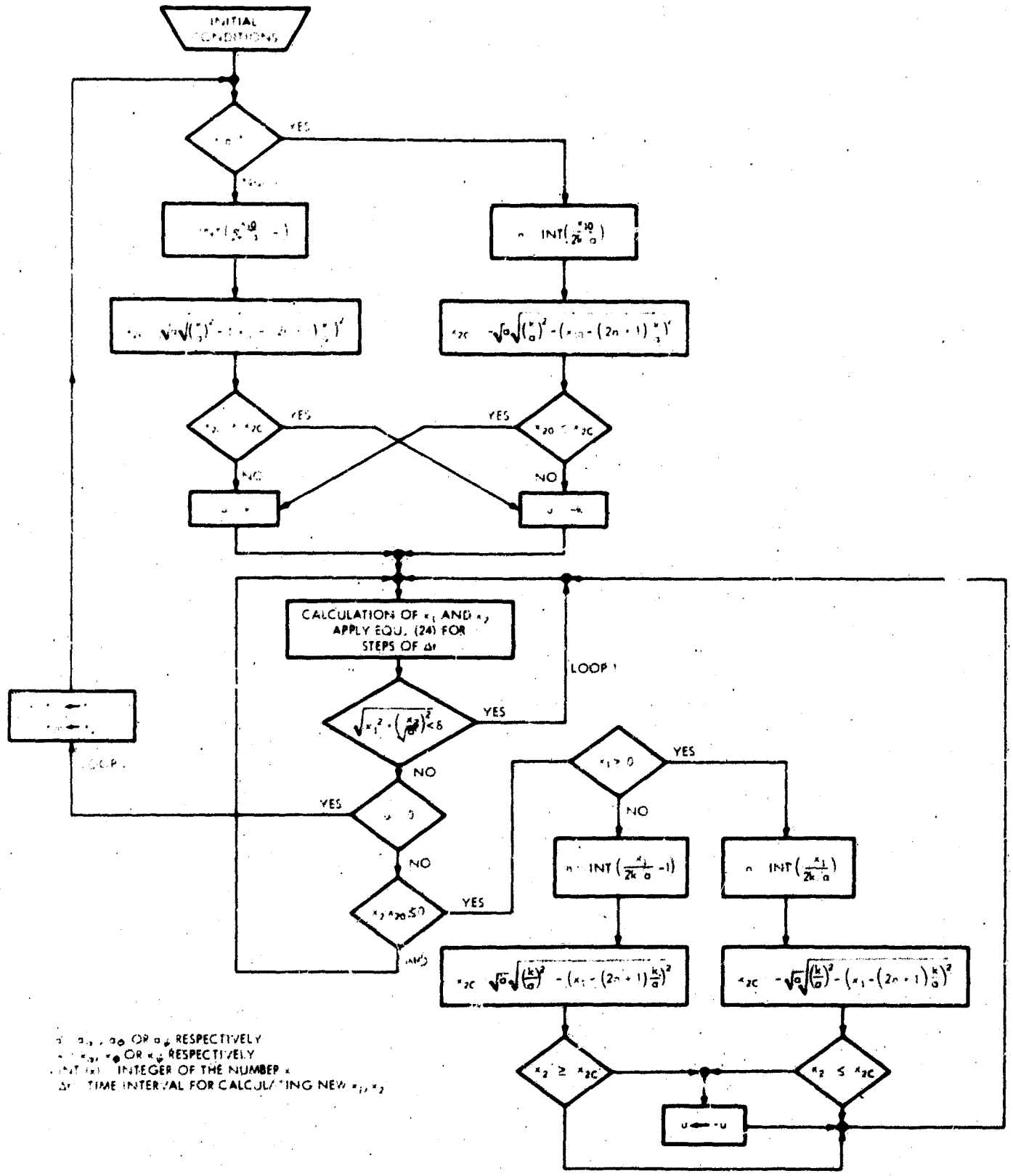

Figure 4–Simplified flowchart for trajectories with optimal control according to Fig. 3 for gravity gradient coefficients a_α, a_ϕ, $a_\psi \neq 0$.

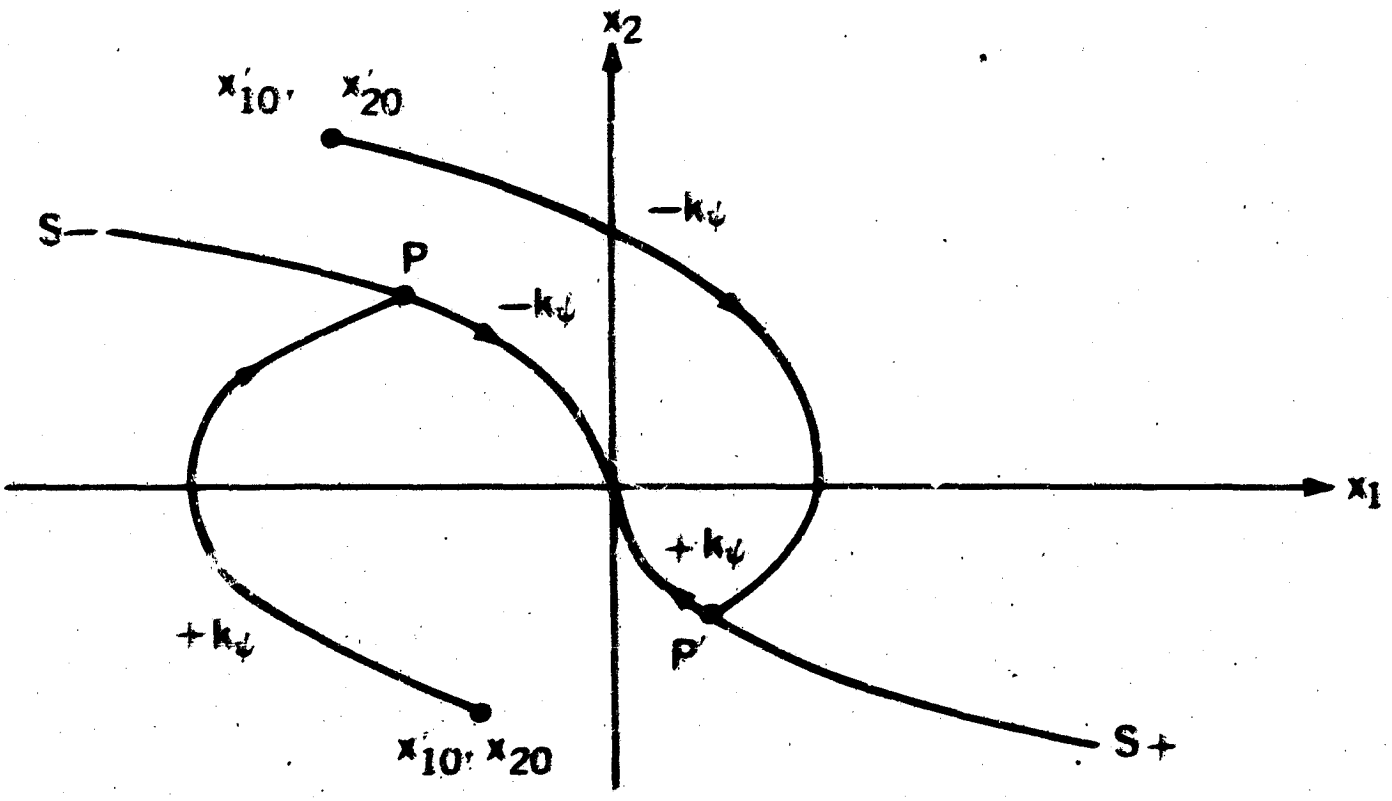

Figure 5–Switching lines S_+ and S_- for optimal control of $x_1 = \cdot$ and $x_2 = \cdot$ in the case of $a_\cdot = 0$. Two examples of optimal trajectories are shown with switching points P and P' respectively. S_+ is given by $x_2 = - \overline{2K_\cdot \cdot}$, S_- by $x_2 = + \overline{2K_\cdot \cdot}$.

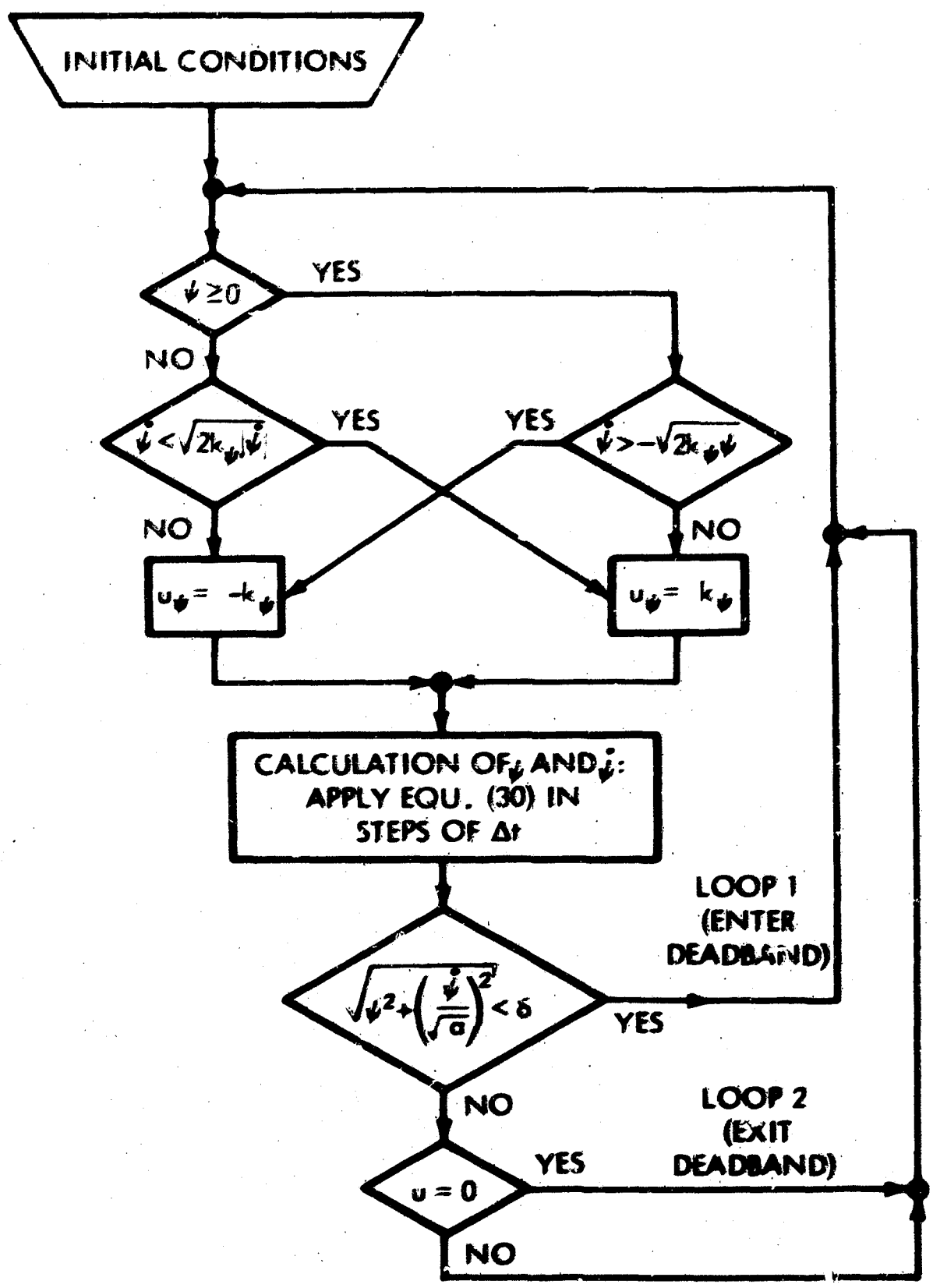

Figure 6—Simplified flowchart for optimal control of yaw (ψ) for $a_\psi = 0$ using the scheme presented in Fig. 5. Similar explanations hold as for Fig. 4.

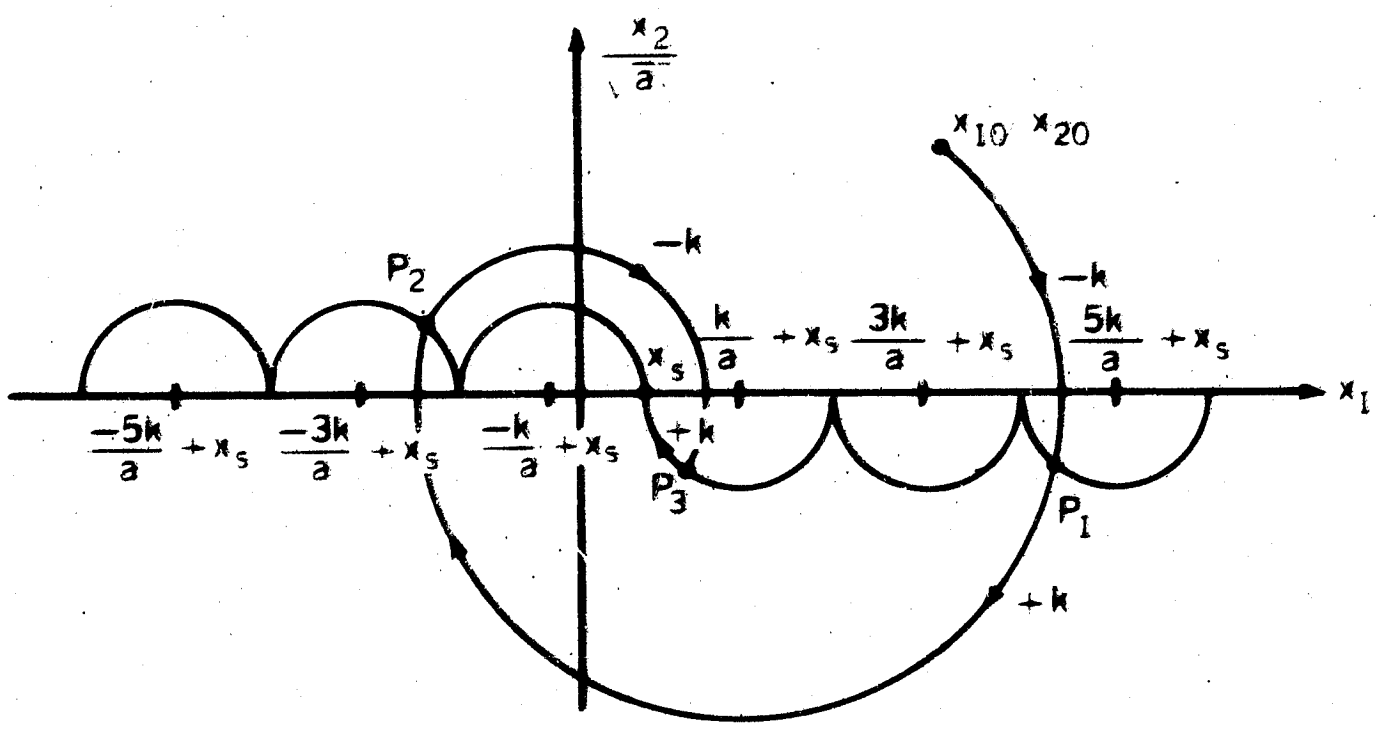

Figure 7–Switching lines and optimal trajectories for $x_1 = x$, $\dot{x}$ or v and $x_2 = \dot{x}$, $\ddot{x}$ or $\dot{v}$ respectively. Also $(a, K) = (a_x, K_x)$, $(a_{\dot{x}}, K_{\dot{x}})$ or $(a_{\ddot{x}}, K_{\ddot{x}})$ respectively.

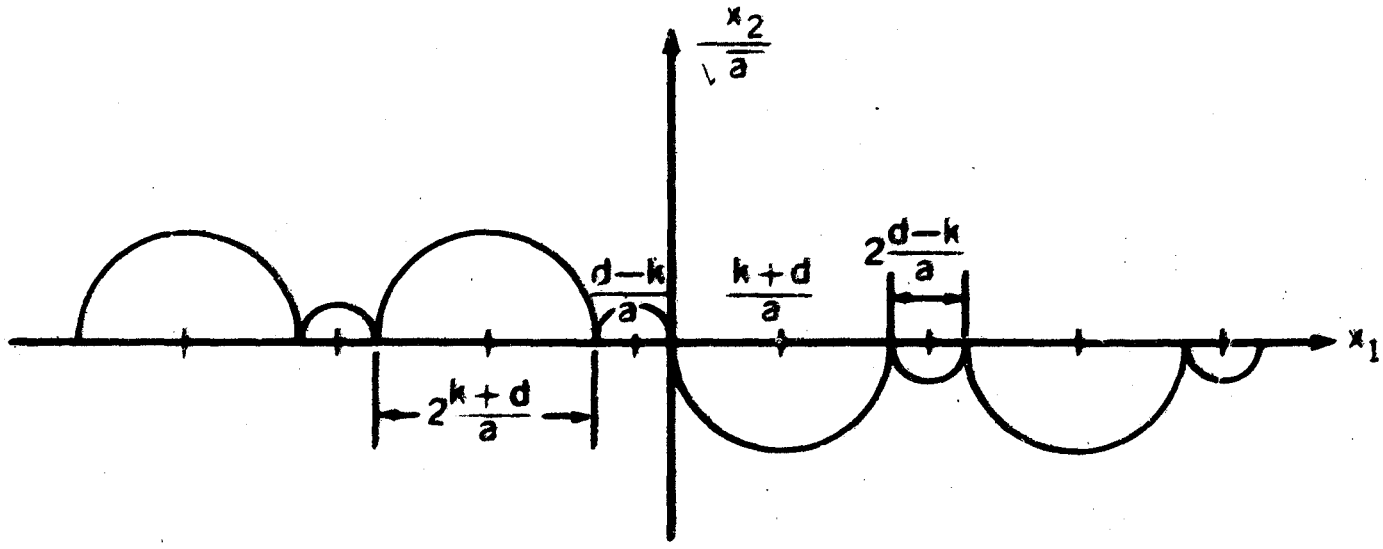

Figure 8–Switching lines for optimal control of α, β or γ in the case of a_α, a_β or $a_\gamma = 0$, respectively, and in the presence of a constant disturbance torque $x_3 = \alpha$, β or γ, γ; α, β or γ, $K = K_\alpha$, K_β or K_γ, $a = a_\alpha$, a_β or a_γ and $d = d_\alpha$, d_β or d_γ respectively.

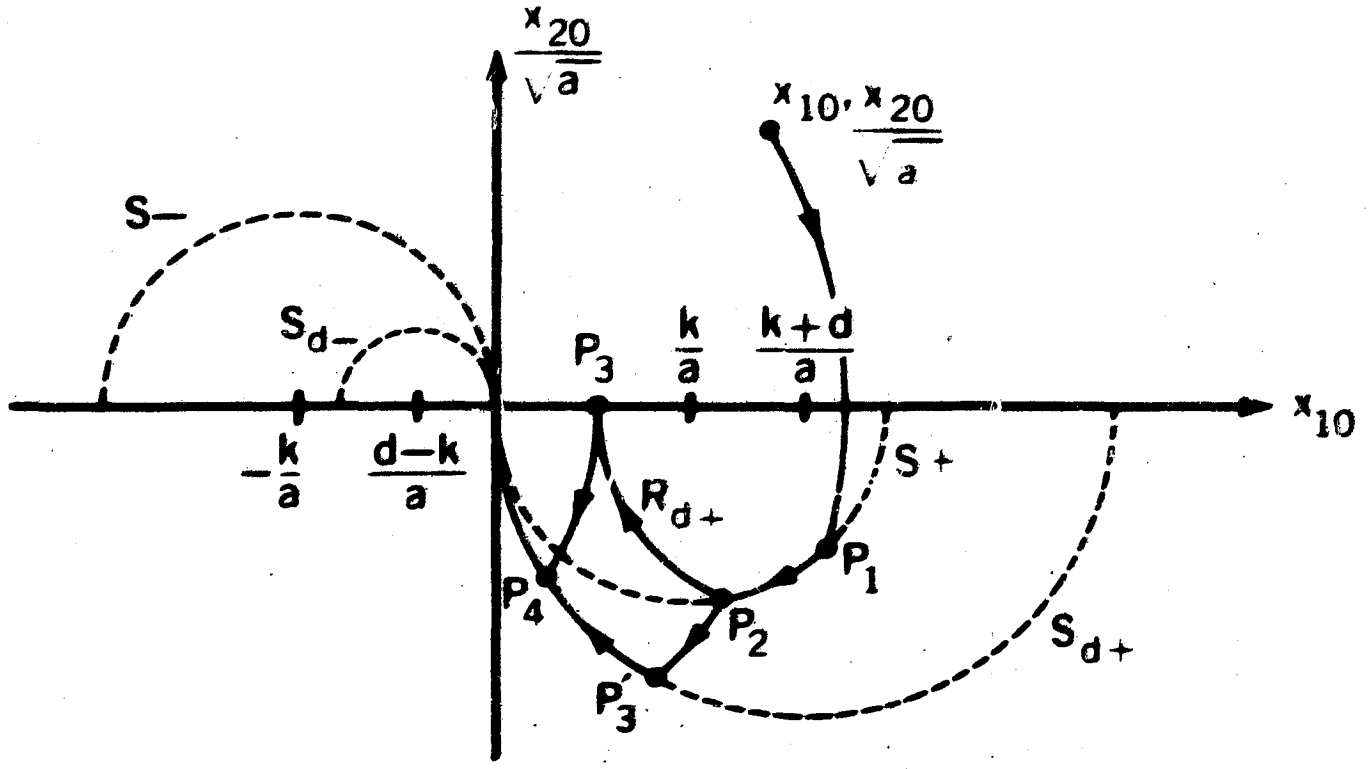

Figure 9–Optimal trajectories under the influence of changing disturbances. The optimal trajectory starts at $(x_{10}, x_{20}, \bar{a})$ without disturbance. A disturbance d occurs when the state is at P_2. The switching lines S_+ and S_- are then replaced by S_{d+} and S_{d-} respectively. Two possible control procedures that lead the state to the origin are: (a) a policy that yields the path P_2, P_3, P_4, origin, or (b) a policy that yields the path P_2, P_3', P_4, origin. For K, a, d, x_1 and x_2 see Fig. 8.

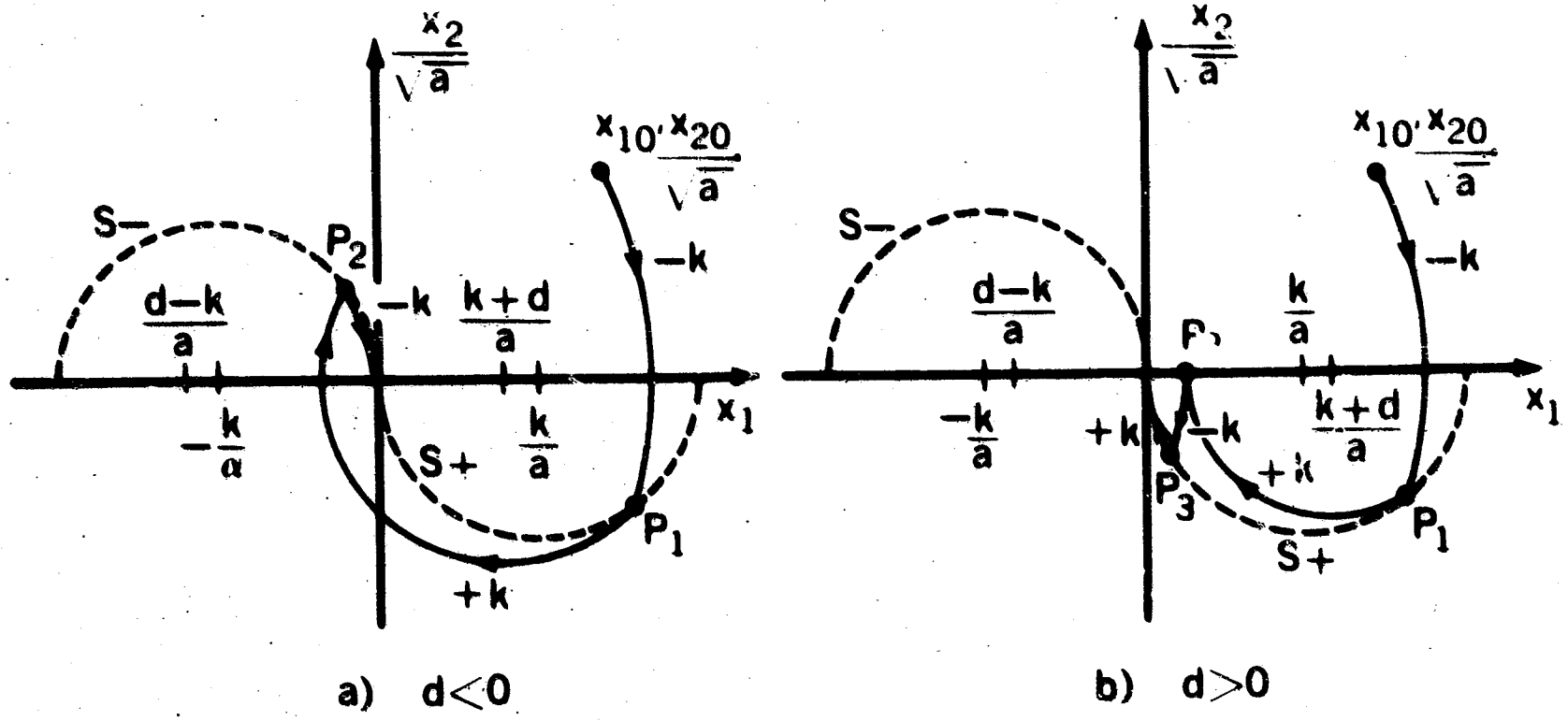

Figure 10–Trajectories in the presence of small disturbances with switching lines as in Fig. 3. Even with these unchanged switching lines the vicinity of the origin is reached fast. P_i – switching points. For K, a, d, x_1 and x_2 see Fig. 8.

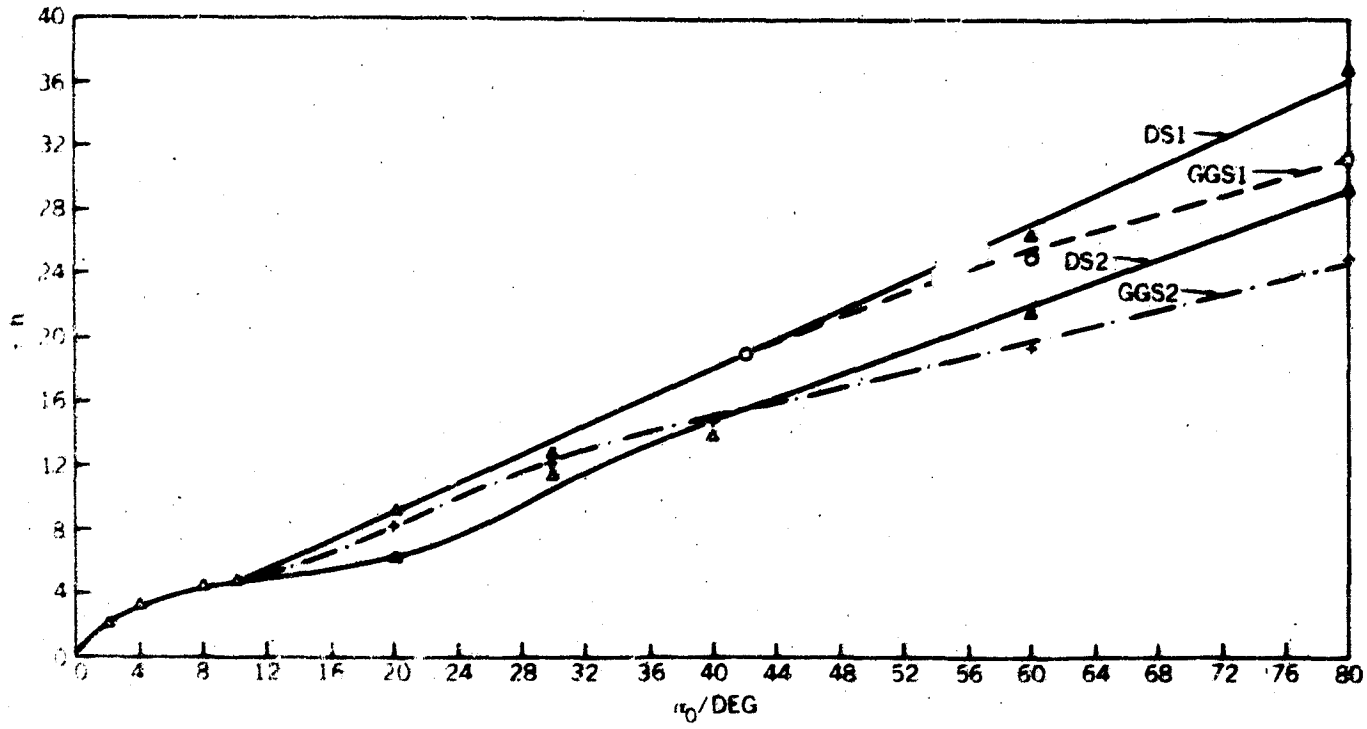

Figure 11–Comparison of time consumed (τ) for damping of initial pitch angles (α_0) to 0°. The initial conditions on roll (ϕ_0) and yaw (ψ_0) are 0°, $\dot{\alpha}_0 = \dot{\phi}_0 = \dot{\psi}_0 = 0$.

- GGS 1 -- GGS with two principal moments of inertia equal
- GGS 2 – GGS with all principal moments of inertia different
- DS 1 – Dumbbell satellite with a_τ and K_α as GGS 1
- DS 2 – Dumbbell satellite with a_α and K_τ as GGS 2

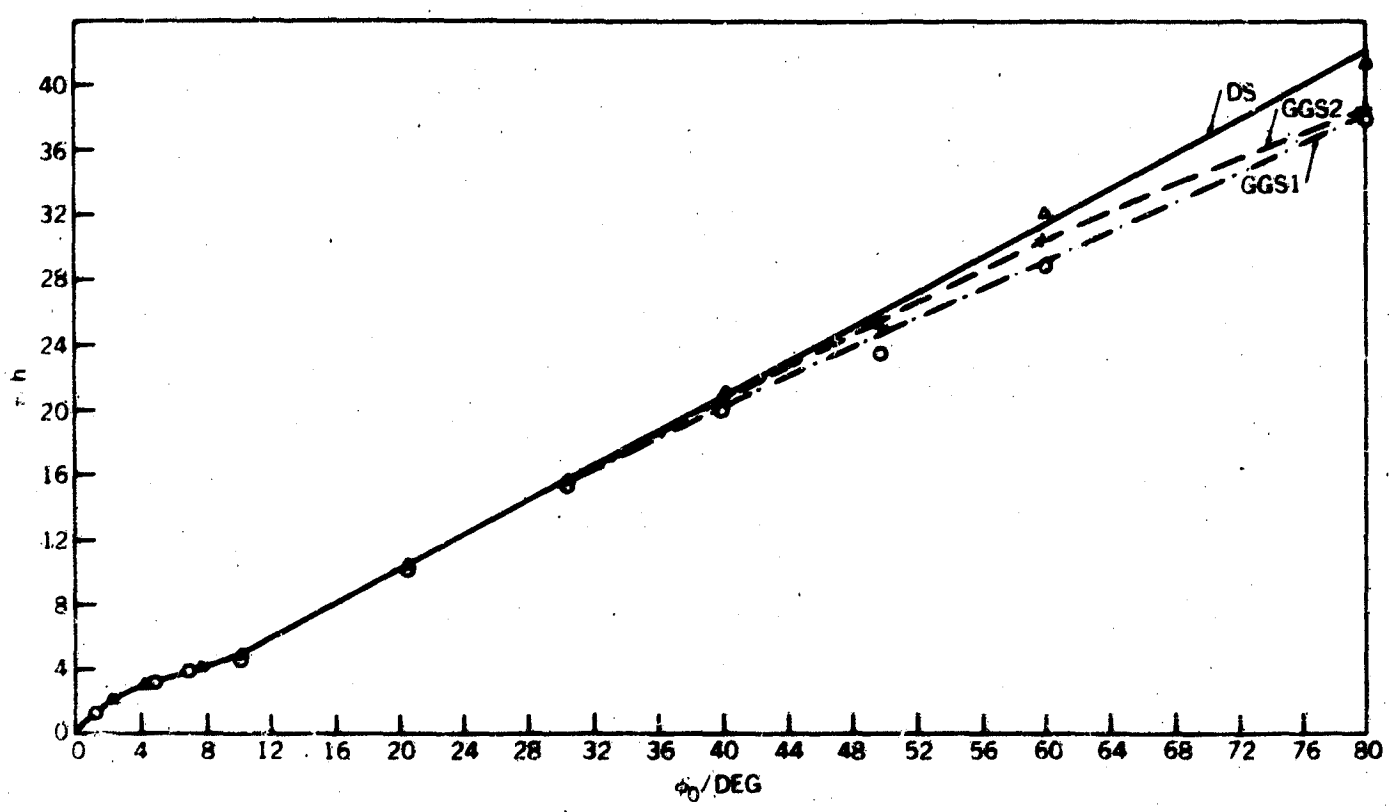

Figure 12--Comparison of τ for damping of initial roll angles (ϕ_0) to 0°. The other initial conditions are: $\alpha_0 = \beta_0 = 0$, $\dot{\alpha}_0 = \dot{\phi}_0 = \dot{\psi}_0 = 0$. σ_ϕ and K_ϕ are equal for both GGS and therefore the same DS is applied for comparison.

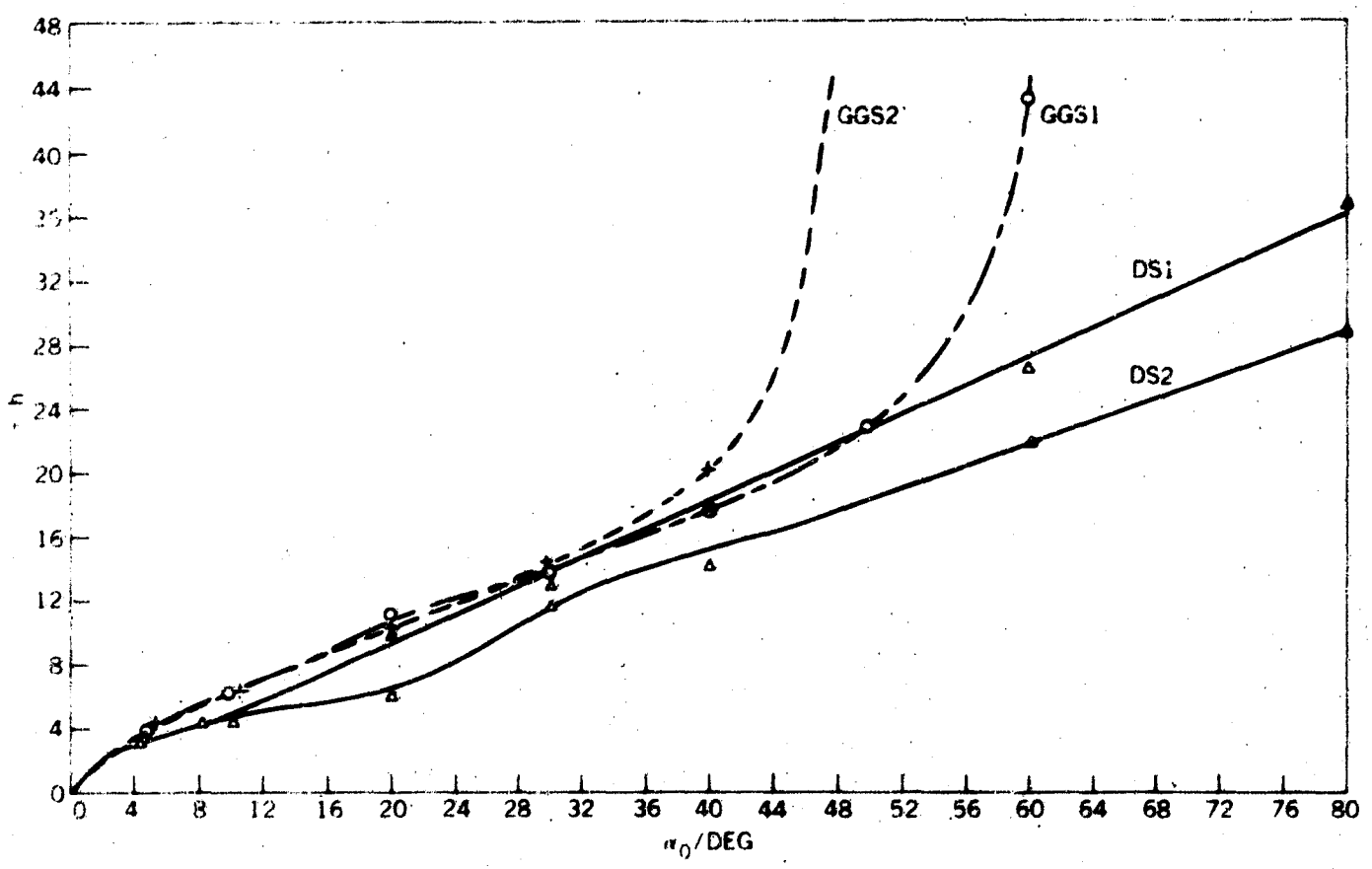

Figure 13–Comparison of τ for damping of initial pitch angles (α_0) to 0° considering initial conditions on the other axes not equal to 0°. The other initial conditions are $\phi_0 = \psi_0 = \alpha_0$, $\dot{\alpha}_0 = \dot{\phi}_0 = \dot{\psi}_0 = 0$. DS 1 again is for comparison with GGS 1, DS 2 for comparison with GGS 2.

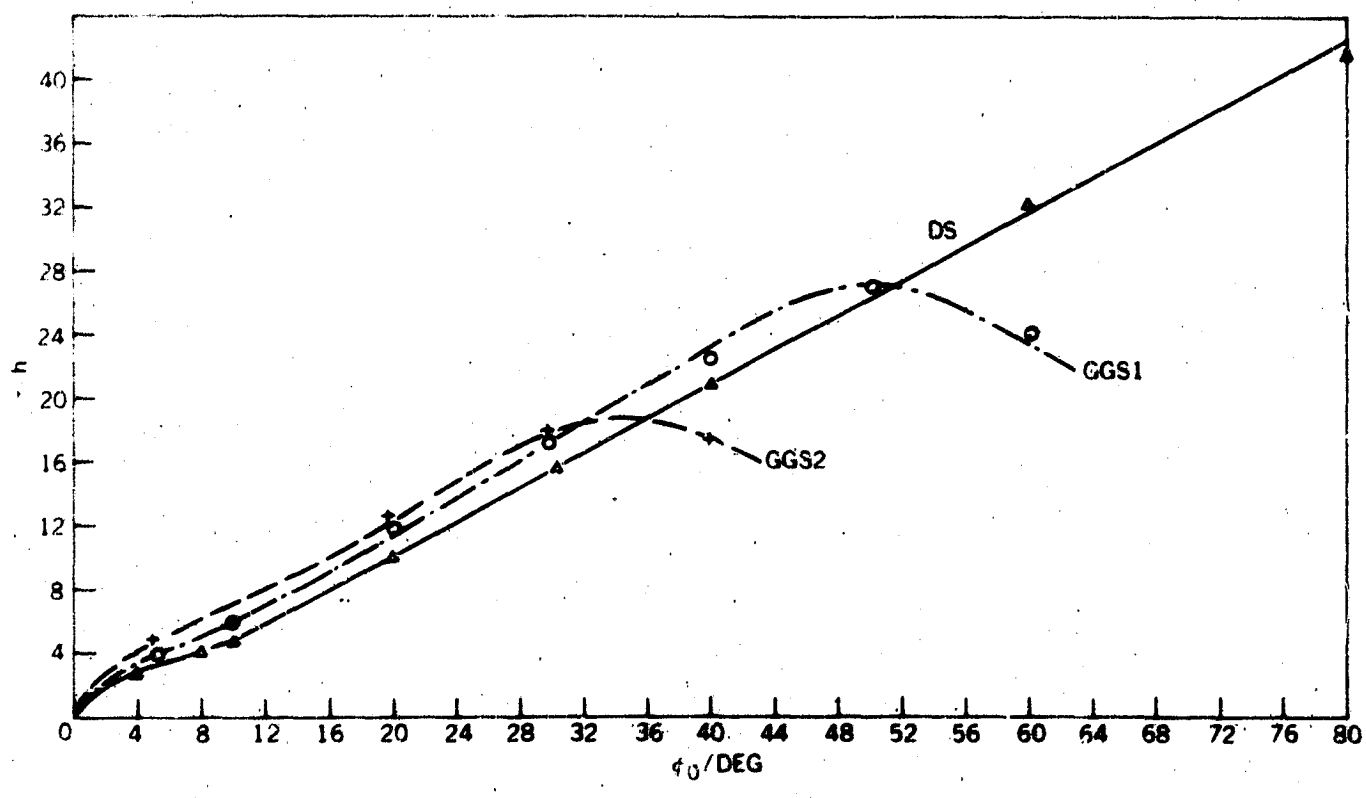

Figure 14–Comparison of τ for damping of initial roll angles (ϕ_0) to 0° with initial conditions on the other axes not equal to 0°. These other initial conditions are $\alpha_0 = \psi_0 = \phi_0$, $\dot{\alpha}_0 = \dot{\phi}_0 = \dot{\psi}_0 = 0$. Both GGS 1 and GGS 2 can be compared with the same DS.

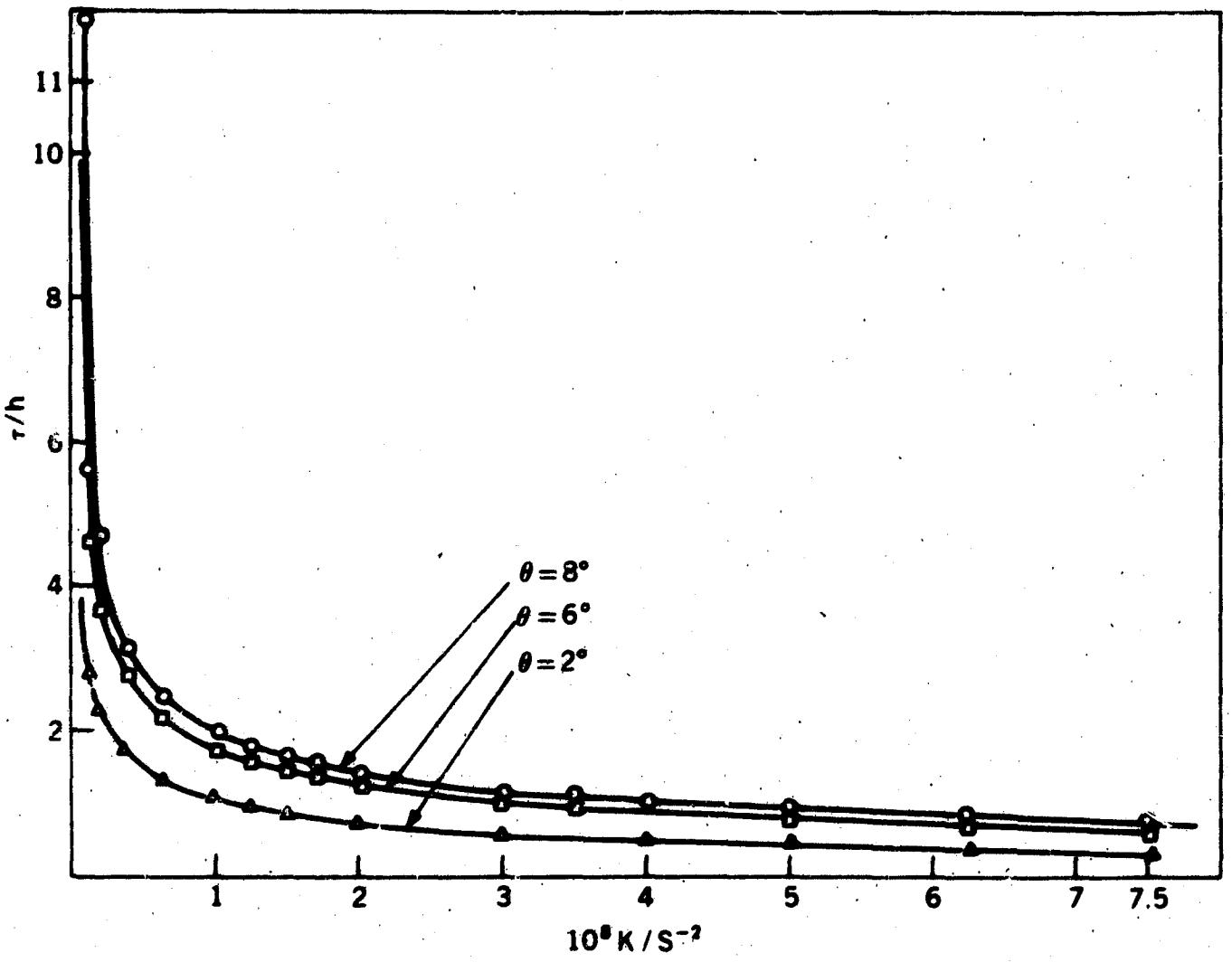

Figure 15–Time consumed by a DS for changing the direction of pointing by $\Theta = 2°$, 6°, and 8° as a function of the reduced torque $K = T_c / I$.

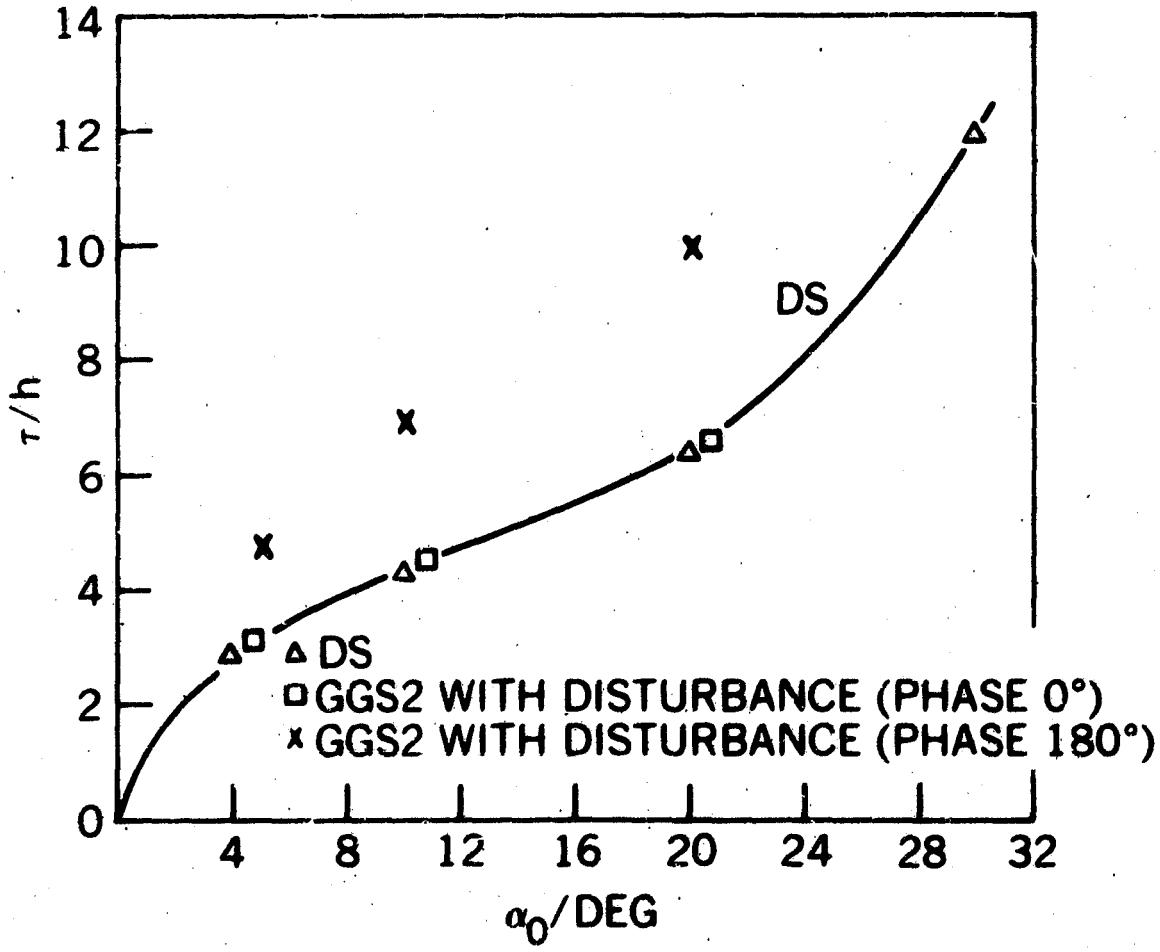

Figure 16–Influence of disturbances on τ for initial pitch angles for GGS 2. $t_0 = \psi_0 = 0$, $\dot{\alpha}_0 = \dot{t}_0 = \dot{\psi}_0 = 0$. The disturbances are sinusoidal with a peak value of 10^{-5} ft lb, a period of 24 hours and a phasing of 0° relative to the start of the control in the first case and 180° in the second case.

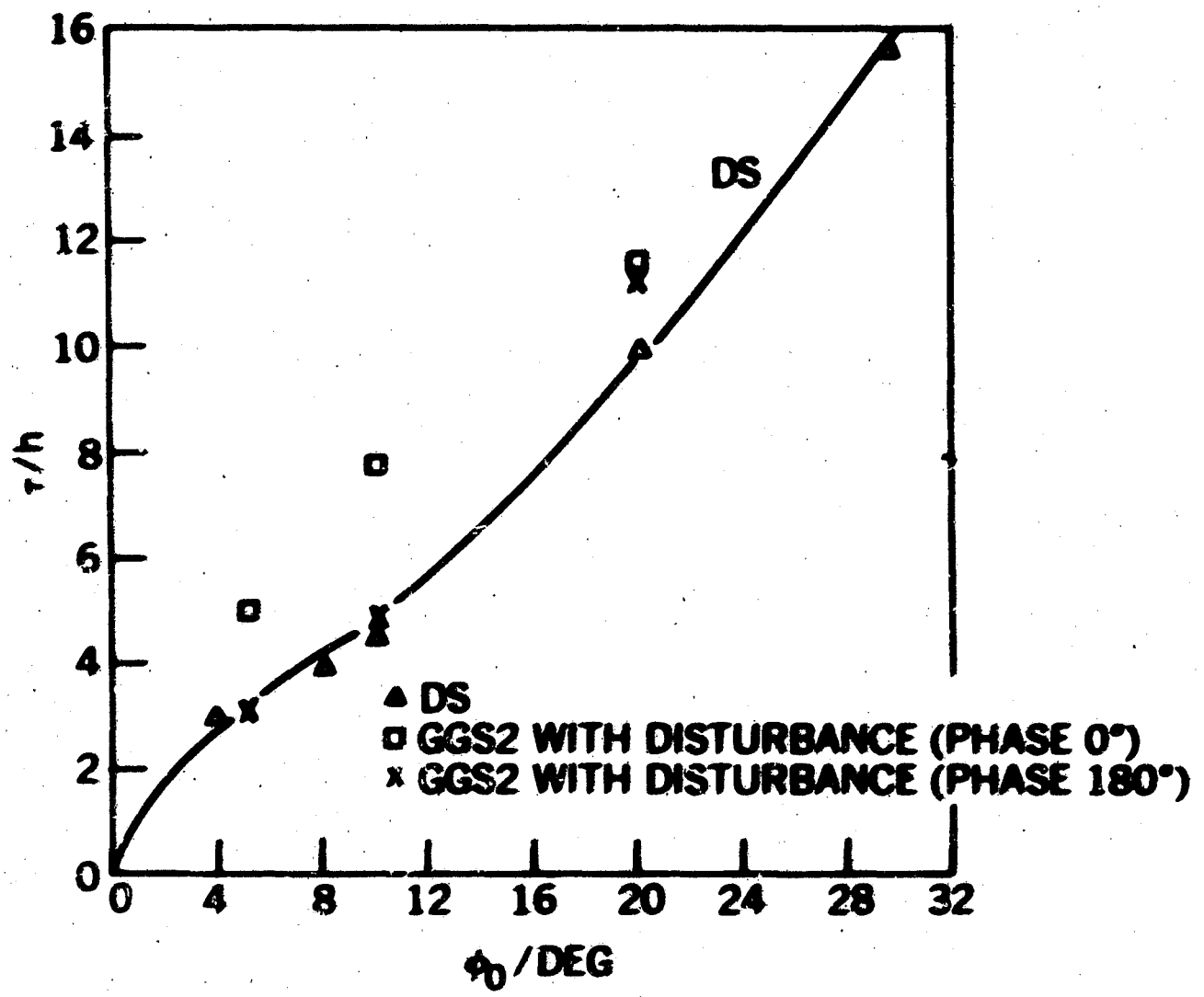

Figure 17–Influence of disturbances on τ for initial roll angles for GGS 2. $\alpha_0 = \psi_0 = 0$, $\dot{\alpha}_0 = \dot{\beta}_0 = \dot{\psi}_0 = 0$. The disturbances are the same as for Fig. 16.